JOURNAL OF PROPULSION AND POWER
Vol. 17, No. 3, May–June 2001

# Tip Leakage Flow in a Radial Inflow Turbine with Varying Gap Height

R. Dambach* and H. P. Hodson†
*University of Cambridge, Cambridge, England CB3 0DY, United Kingdom*

**Tip leakage flow in a radial inflow turbine is investigated for two different uniform clearances of 0.6 and 1.2% of span. The clearances are typical of radial turbines for industrial applications. Measurements were also performed for increased axial clearances (6 and 7% of span), while the radial clearance was kept constant. Static pressure and hot-wire measurements in the gap region confirmed an earlier finding by the authors that the tip leakage flow behaviour in a radial turbine is interdependent with the scraping flow. Changes in the nature of tip leakage flow with increasing tip clearance height seem mainly to occur in regions where the scraping effect is important. The mass flow over the tip of the present radial inflow turbine was quantified for all four clearance configurations. The measurements revealed that the relative casing motion drags an approximately constant amount of scraping fluid from the suction side to the pressure side irrespective of the gap height, if the tip gap height to width ratio is above a critical value. The modeling of the effect of scraping in the inducer seems necessary if a successful prediction of the mass flow and, hence, loss is attempted in the future.**

## Nomenclature

| | | |
|---|---|---|
| $C_D$ | = | discharge coefficient |
| $C_p^*$ | = | reduced static pressure coefficient |
| $M$ | = | momentum |
| $\dot{m}$ | = | mass flow rate |
| $p$ | = | static pressure |
| $p_0$ | = | stagnation pressure |
| $p^*$ | = | reduced static pressure, $p - \frac{1}{2}\rho U^2$ |
| $R$ | = | scraping ratio |
| $S$ | = | blade length |
| $S_m$ | = | meridional length |
| $s$ | = | span (blade height) |
| $t$ | = | tip gap height ($z$-axis) |
| $U$ | = | blade speed |
| $v$ | = | velocity |
| $w$ | = | blade thickness ($y$-axis) |
| $\gamma$ | = | local blade angle (camber line) |
| $\theta$ | = | circumferential coordinate |
| $\lambda$ | = | tip gap height-to-width ratio, $t/w$ |
| $\rho$ | = | density |

*Subscripts*

| | | |
|---|---|---|
| $n$ | = | blade normal |
| $p$ | = | passage |
| sf | = | scraping flow |
| tf | = | pressure driven tip leakage flow |
| 3 | = | rotor inlet |

## Introduction

THE tip leakage flow in radial inflow turbines is different from that in axial flow turbines. The stage efficiency of radial turbines generally suffers less from an increase in tip clearance than that of axial turbines. Tests undertaken on various rig facilities showed that there is about a 1% penalty on radial turbine efficiency for each 1% increase in tip clearance[1–3] (see also Japikse and Baines[4] for a brief overview). In the case of axial turbines, Sjolander[5] suggests that there is on average a 2% decrease in stage efficiency for each 1% increase in tip clearance height.

Dambach et al.[6] have indicated that the different efficiency gradient for tip leakage losses is due to the effect of the relative casing motion on the tip leakage flow in radial turbines. Scraping flow (flow that adheres to the casing in the relative frame) interacts with the tip leakage flow (driven by the over-tip pressure difference) near the tip gap on the suction side. The two flows oppose each other in a turbine. Because most studies of tip leakage flow in axial turbines have been undertaken without considering the relative casing motion, relatively little is known about the scraping effect. It is generally argued that the relative casing motion has a negligible effect on leakage flow in an axial turbine, although some authors admit the need to collect more data in rotating test rigs (e.g., Yaras and Sjolander[7] and Kaiser and Bindon[8]). Therefore, it is not surprising that the scraping effect on tip leakage flow in radial turbines was only considered relatively recently.

Dambach et al.[6] have shown that in the case of a radial turbine the relative casing motion can no longer be neglected because of the comparatively large tip radius at inlet to the rotor. Figure 1 shows a schematic of velocity components near the casing in the tip region of the present turbine. All velocity components are drawn to scale for the design flow coefficient. The blade normal component of tip leakage flow was calculated from the pressure difference at 90% span. The blade parallel component of velocity on the pressure side is the isentropic velocity at 90% span. The casing is moving with the blade tip speed $U$ in the tangential direction.

According to Fig. 1, Dambach et al.[6] have divided the tip leakage flow in a radial turbine into three regions. Near the leading edge, the blade tip speed is large, and hence, the relative casing motion normal to the blade is important [radial turbine blades at inlet are often radial (i.e., $\gamma = 0$) for structural reasons]. Hence, in the first region (the inducer) the tip leakage flow near the casing is opposed by a large scraping flow component. As the flow moves toward the trailing edge, three changes occur. First, the relative casing motion decreases with decreasing radius. Second, the blade normal component of scraping flow becomes less important as the local blade angle at the tip begins to increase. Third, the tip leakage velocity becomes stronger as the blade loading over the tip increases (as observed in Fig. 1). Measurements have shown that all of these three changes reduce the strength of the scraping flow relative to the tip leakage flow.

On the basis of these measurements, Dambach et al.[6] introduced the concept of a scraping ratio defined as

$$R = \frac{\Delta p_{\text{over-tip}}}{\frac{1}{2}\rho U^2 \cos^2 \gamma} \tag{1}$$

Received 17 December 1999; revision received 10 May 2000; accepted for publication 8 August 2000. 

*Assistant Director, Engineering Turbines, Cryostar France (Member of the British Oxygen Company), Zone Industrielle, 68220 Hésingue, France.
†Reader in Thermofluid Engineering, Whittle Laboratory, Department of Engineering, Madingley Road.

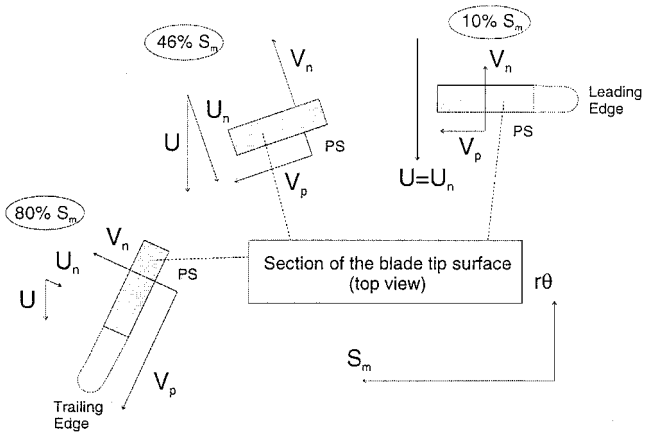


**Fig. 1 Projection of a stream surface showing the important parameters for tip leakage flow.[6]**

where $\Delta p_{\text{over-tip}}$ is the driving pressure difference over the blade tip. They reported that for $R < 1$ scraping fluid is dragged through the gap, whereas for $R > 1$, the dragged scraping layer inside the gap could not be captured anymore.

The objectives of this paper are to investigate the tip leakage flow and to understand the scraping effect for a large clearance variation and to quantify the mass flow rate over the tip.

## Experimental Apparatus

The experiments were performed in a large-scale, low-speed radial inflow turbine. Air at atmospheric conditions is drawn through the turbine by a centrifugal fan. The mass flow rate is controlled by a throttle situated downstream of the turbine. Figure 2 shows a schematic of the radial inflow turbine. The test facility has been described in detail by Huntsman and Hodson.[9,10]

All measurements were performed at the design condition as described by Huntsman and Hodson.[9] The tip flow was examined at seven different chordwise positions and four different gap heights. Table 1 summarizes the most important parameters for this particular study in the tip gap region.

The tip gap height of the radial inflow turbine was designed to be a uniform percentage of the local blade height (0.6% of span). All previous investigations have been conducted with this clearance. As part of the present investigation, the clearance was increased from 0.6 to 1.2% of span by modifying the blade tips. To increase the axial clearance only, a similar approach to that of Futral and Holeski[1] was chosen. Shims were located between the rotor casing and the radial section containing the nozzles. The location of the shims in the present study resulted in moving the shroud wall of the rotor, thus introducing a backward-facing step in the interspace between the stator and the rotor.

Because this paper compares tip leakage flow measurements with and without shims, the effect of the shims on the flow through the rotor is briefly addressed. Roelke and Rogo[11] tested the change in overall performance when moving the shroud wall of the nozzle guide vanes. This procedure introduced an axial step between the stator and rotor shrouds similar to the setup in the present facility, but without increasing the axial clearance of the rotor. According to Roelke and Rogo,[11] the change in efficiency from the peak value to the value at 50% nozzle flow area was approximately 3.5%. Assuming a linear behavior, inserting eight shims (total thickness of 8 mm) in the present test rig would contribute to about 0.45% loss of overall efficiency (for a nozzle area increase of 5.9%), due to the step alone. This is about $\frac{1}{6}$th of the measured loss of overall efficiency for the same increase in axial clearance.

The four different gap configurations together with the labeling convention adopted for the paper are summarized in Fig. 3. Gap A0 indicates the design clearance of 0.6% of span and gap A8 is the same clearance with eight shims inserted. Gaps B0 and B8 indicate the clearance of 1.2% of span with zero and eight shims inserted, respectively.

**Table 1 Leading parameters for the test section at the design point**

| Parameter | Value |
|---|---|
| Rotational speed | 450 rpm |
| Mass flow rate | 4.5 kg/s |
| No. of rotor blades | 14 |
| Average blade normal thickness at the tip | 8 mm |
| Meridional chord at the casing | 460 mm |
| Rotor inlet radius | 609 mm |
| Rotor exit radius at the tip | 445 mm |
| Rotor inlet angle (mean flow) | −18.4 deg |
| Rotor exit angle at the tip (mean flow) | −72 deg |
| Pressure side tip corner radius | 0.25 mm |

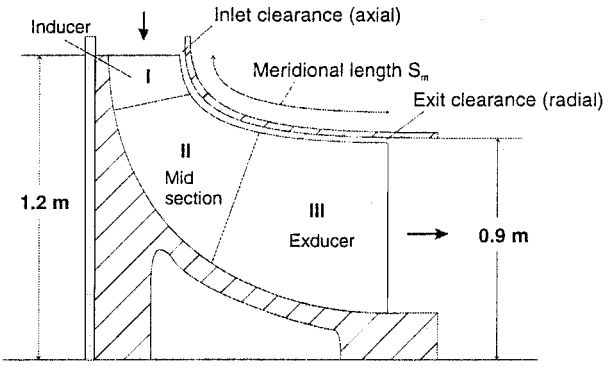


**Fig. 2 Schematic of the radial inflow turbine test facility.**

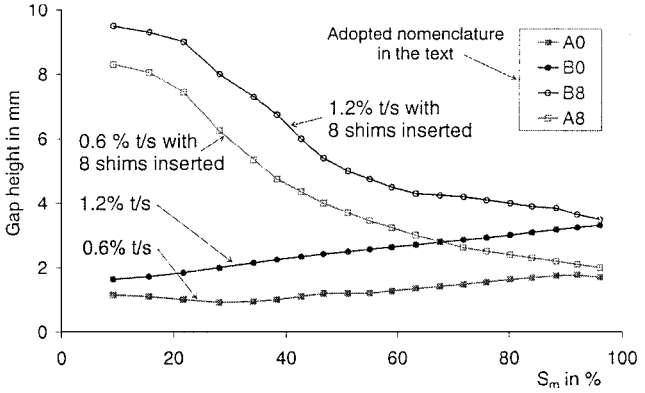


**Fig. 3 Tip gap height for four clearance configurations.**

## Experimental Techniques

### Static Pressure Measurements at the Rotor Casing

The static pressure at the casing was measured at 21 locations between 9 and 100% of meridional blade length. The pressure tappings were located at a nominally constant $\theta$ value. The logging of the static pressure data was triggered by a once per revolution trigger pulse. The time-mean, steady-state pressure level was obtained using a Scanivalve pressure switch. The unsteady pressure variation was measured with a Kulite XCS062 pressure transducer in the same location (frequency response of 125 kHz). Between 18 and 23 measurements were taken over the width of the blade. The fluctuating pressure (ac coupled) was subsequently added to the steady pressure for each pressure tapping and ensemble averaged over 50 passages.

### Hot-Wire Traverses into the Tip Gap

A single axis hot wire was employed in the gap region to examine the flowfield between the blade tip and the casing. The hot wire was mounted upon a two-axis traverse gear, which allowed the sensor to turn around its own axis and to move into the gap in the spanwise

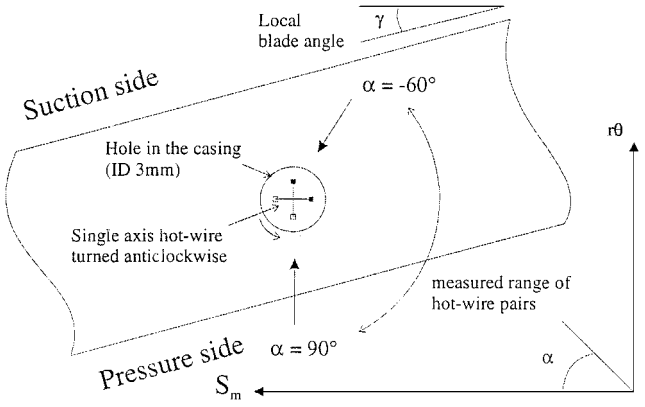


**Fig. 4 Rotation of the single axis hot wire above the blade tip.**

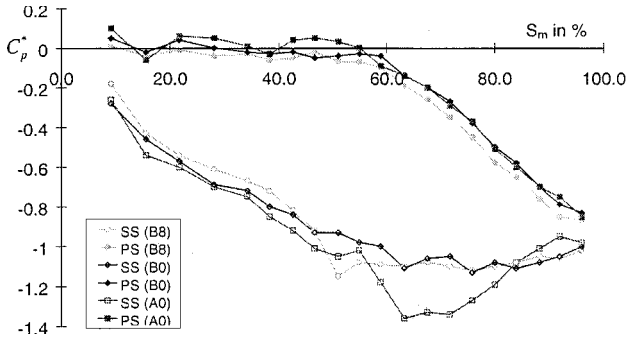


**Fig. 5 Reduced static pressure coefficient at the casing.**

direction. These traverses were performed at 9, 21, 34, 46, 58, 71, and 88% of meridional blade length. Hot-wire traverses into the gap consisted of 33 points in the radial direction and about 40 points across the width of the blade (frequency response of 125 kHz). Where the gap height exceeded 4 mm, up to 52 radial points were measured. A measurement was triggered once per revolution, and the traces were ensembled over 80 rotor cycles. At each radial immersion, the hot-wire was rotated around its axis to six different angular positions ranging from $\alpha = 0$ (hot wire in the direction of the meridional vector) to $\alpha = 150$ deg, as indicated in Fig. 4. The six sensor positions formed three different pairs. To deduce the absolute flow angle, the two hot-wire pairs were chosen with most equal velocity readings, and the angle was calculated with a linear blending function. The velocity magnitude was deduced from the hot-wire position most perpendicular to the absolute flow angle, once the flow angle was known.

#### Errors due to Calibration, Data Acquisition and Processing

Errors due to calibration and signal randomness introduce an uncertainty, especially when transforming the measured absolute velocities into the relative frame. At $S_m = 21\%$, where the absolute tip flow angle was close to 90 deg, the maximum error on the relative velocity inside the gap was $\pm 4\%$ of the local tip speed, and the maximum error on the relative angle was $\pm 10$ deg. For all other measurement locations, the error on the relative velocity was less than $\pm 3\%$ of the local tip speed, and the error on relative angle was less than $\pm 4$ deg.

The tangential resolution guaranteed that the error due to spatial averaging was negligible inside the tip gap region. Outside the gap region, where steep velocity gradients occurred, a maximum error of 8% of the blade speed was estimated due to spatial averaging.

## Results and Discussion

In the following, the flow features of tip leakage flow for varying gap height are analyzed. First, the driving pressure difference over the tip is investigated for different gap height. The tip leakage flow features are then presented for the inducer, that is, $0\% < S_m < 22\%$, and for the midsection, that is, $22\% < S_m < 60\%$. Hot-wire experiments in the gap region of the exducer, that is, $60\% < S_m < 100\%$, showed that the tip leakage flow pattern did not change significantly with varying gap height in this region. For the sake of brevity, results in the exducer are not presented here. A theory is proposed to explain the different tip leakage flow behavior for varying gap height. Finally, the tip gap mass flow is quantified.

#### Pressure Distribution in the Tip Gap Region

One of the aims of studying the effect of varying tip gap height on the tip leakage flow in a radial turbine was to keep all other tip leakage parameters constant. Figure 5 shows the loading distribution for three different tip gap configurations. No pressure measurements are available for gap A8. To present the data Dambach et al.[6] defined the reduced static pressure coefficient

$$Cp^*_{\text{static}} = \frac{p^* - (p_{03} - \rho U_3 V_{\Theta 3})}{\frac{1}{2}\rho U_3^2} \tag{2}$$

To obtain Fig. 5, the minimum and maximum pressures were taken from the ensembled data of the 20 different static pressure traces. All values were averaged over three blade passages. The minimum and maximum pressures were not necessarily located at the suction side or on the pressure side. The location of the maximum pressure did extend as far upstream of the gap as $y/w = 3$, where $y/w$ is the fraction of blade thickness, that is, $y/w = 0$ at the suction side and $y/w = 1$ at the pressure side.

Figure 5 shows that for the present purpose the imposed loading at the casing (and hence the driving mechanism for tip leakage flow) was not significantly altered for a large variation of the tip gap height. This is especially significant in the inducer, where the clearance changed by a factor of 5–7 (see Fig. 3). As far as is known, such a result has never been reported for the case of rotating turbines. A similar result was reported from linear cascade work by Sjolander and Amrud[12] and Bindon.[13] Bindon[13] indicated that the pressure changes at the pressure side corner of the blade, but that the bulk of the mass flow appears to experience the same driving pressure difference for a variety of clearances.

The preceding result has important implications for the modeling of the tip gap mass flow because Dambach et al.[6] showed that the pressure loading at 90% span is very similar to that at the casing. It means that the over-tip pressure difference, which is fed into a tip gap mass flow model, can be simulated by an Euler calculation without tip clearance.

#### Tip Leakage Flow Pattern in the Inducer

Figure 6 shows blade normal velocity vectors at 21% $S_m$, that is, in the inducer, for three different gap heights. It can be observed that much scraping fluid is dragged from the suction side to the pressure side in the case of the smallest gap A0. As the gap height is increased (drawings are not to scale), the scraping flow occupies less of the gap height. For gap B0, Fig. 6b shows that a third of the gap height is still filled with scraping fluid at $y/w = 1$. The presence of scraping fluid inside the gap results in an area reduction for the tip gap flow, and the tip gap mass flow rate is substantially reduced in this part of the radial turbine. For the biggest gap B8, the scraping fluid only occupies a small proportion of the gap height, as observed in Fig. 6c. Nevertheless, the dragging effect of scraping remains present because $R$ is smaller than 1 ($R = 0.7$).

Figure 7 shows the static pressure at the casing for the different gap heights. Dambach et al.[6] reported that the pressure drop for gap A0 that takes place outside the gap near the suction side is related to the stagnating scraping flow (in accordance with an earlier argument by Rains[14]). This was confirmed by the blade normal velocity vectors (see Fig. 6a), which showed that the scraping momentum was reduced near $y/w = 0$. As the gap height was increased in the present project, more tip leakage flow passed through the gap. For gap B0, Fig. 7 shows that the pressure begins to drop

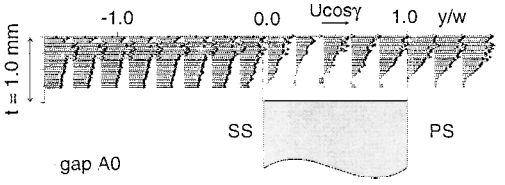


a) Gap A0, 0.6% *t/s*

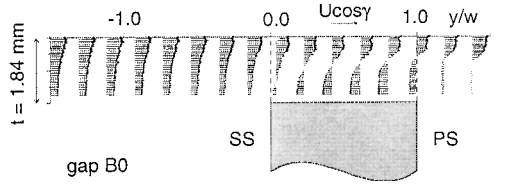


b) Gap B0, 1.2% *t/s*

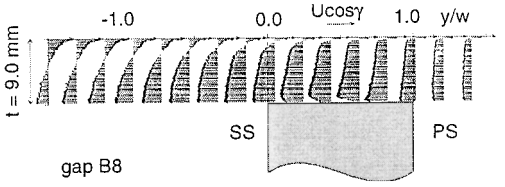


c) Gap B8, 5.9% *t/s*

**Fig. 6 Blade normal velocity vectors determined from hot-wire measurements at 21% $S_m$.**

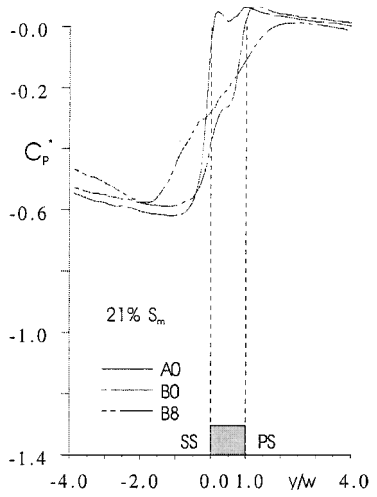


**Fig. 7 Reduced static pressure coefficient at 21% $S_m$.**

at $y/w = 1.25$, and part of the pressure drop is now related to the tip leakage flow. Figure 6b shows that the scraping momentum is approximately constant through the gap. For the biggest gap B8, Fig. 7 shows that the flow begins to accelerate much earlier into the gap. The potential effect of the tip leakage flow extends now to almost two blade thicknesses either side of the blade. A distinct tip leakage jet leaves the gap, as observed in Fig. 6c.

### Tip Leakage Flow Pattern in the Midsection

As the scraping ratio $R$ becomes larger than 1 (at 46% $S_m$, $R = 1.6$), the tip leakage flow begins to dominate over the scraping flow. Figure 8 shows blade normal velocity vectors at 46% $S_m$ for three different gap heights. Dambach et al.[6] showed that the acceleration of the tip leakage flow extends up to the gap exit in the case of gap A0 (see Fig. 8a). They distinguished between a first acceleration of the tip leakage flow into the gap and a second acceleration inside the gap. The second acceleration is caused by the blocking effect of scraping, which is located close to the gap exit for gap A0 (see the dividing stream surface in Fig. 8a). For gaps B0 and B8, Figs. 8b and 8c show, however, that the acceleration is completed soon after entry into the gap.

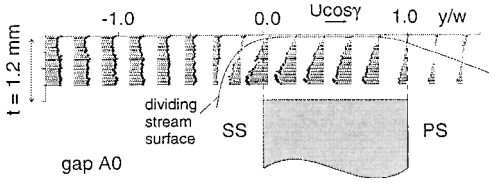


a) Gap A0, 0.6% *t/s*

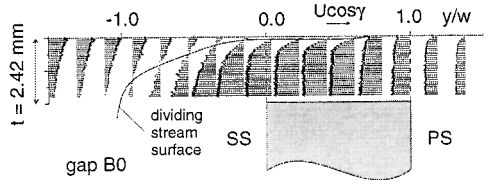


b) Gap B0, 1.2% *t/s*

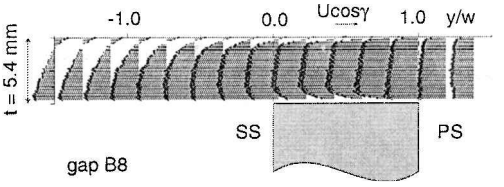


c) Gap B8, 2.7% *t/s*

**Fig. 8 Blade normal velocity vectors determined from hot-wire measurements at 46% $S_m$.**

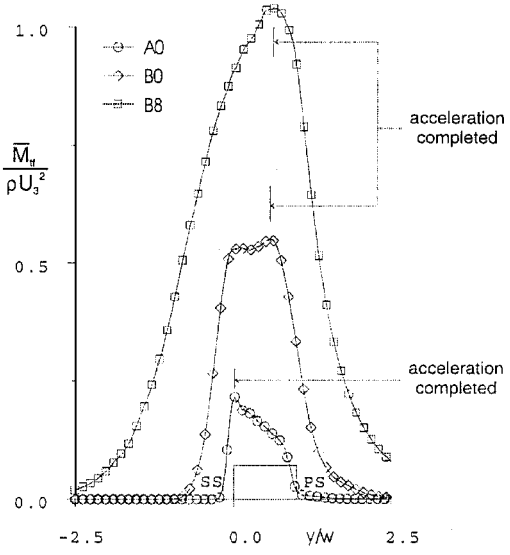


**Fig. 9 Nondimensionalized tip leakage flow momentum at 46% $S_m$.**

The effects noted in Fig. 8 can be more readily observed in Fig. 9, where the tip leakage flow momentum at 46% $S_m$ is displayed. The average tip leakage flow momentum is defined as

$$\bar{M}_{tf} = \frac{1}{t}\int_0^t \rho v_n v_n \, dz \qquad \text{only for} \qquad v_n > 0 \tag{3}$$

where positive $v_n$ is in the direction of the rotation. Figure 9 shows that, for gap A0, the tip leakage flow accelerates up to the gap exit. For the bigger gaps B0 and B8, the acceleration of the tip leakage flow is completed at about $0.6y/w$ (the turning of the flow into near blade perpendicular direction is completed earlier at about $0.8y/w$ for both gaps B0 and B8). Figure 9 also indicates that the second acceleration inside the gap does not occur for gaps B0 and B8. This reveals a fundamental difference in tip leakage flow behavior between gap A0 and gaps B0 and B8.

Figure 8 also shows that some scraping flow is dragged into the gap on the suction side, but most of the scraping flow is blocked off at the gap exit for all three gap configurations. Dambach et al.[6] referred to these two effects as the dragging effect and the blocking

effect of scraping. Little of the dragged scraping fluid leaves the gap on the pressure side, but most of it is diverted by the tip leakage flow inside the gap. Nevertheless, the dragging effect of scraping affects the velocity profile of the tip leakage flow inside the gap. Figure 8a shows a very nonuniform spanwise distribution of the tip leakage flow inside the tip gap ($0 < y/w < 1$). It is believed that this is due to two mixing regions between the tip leakage flow and the scraping flow near the casing and between the tip leakage flow and the boundary-layerflow near the blade tip surface. As the gap height is increased, a more uniform profile for part of the tip leakage flow can be seen in Figs. 8b and 8c. This seems to be another indication that the tip leakage flow pattern is different for gap A0 compared to gaps B0 and B8.

To obtain a qualitative estimate of the mixing process in the gap region of the midsection, rms values from hot-wire measurements are presented in Fig. 10. The rms of the velocity is defined as

$$\mathrm{rms}(\Delta t) = \sqrt{\frac{1}{N}\sum_{n=1}^{N}[V(n, \Delta t) - \hat{V}(\Delta t)]^2} \qquad (4)$$

where $\hat{V}(\Delta t)$ is the ensemble mean of the signal. The measure of random fluctuations in the signal includes those associated with the homogenous isotropic turbulence, as well as any spurious random noise present in the data acquisition system. It is reasonable to assume that the latter remains approximately constant for different experiments and is small. In the following only the component of the rms in the direction of the flow is presented and the rms values are given as a percentage of the local blade tip speed.

For the smaller gap A0, Fig. 10a indicates a strong mixing process inside the upper half of the gap toward the casing. As has been observed in Fig. 8a, this is due to the dragging effect of scraping on the tip leakage flow. In the lower part of the tip gap, tip leakage fluid

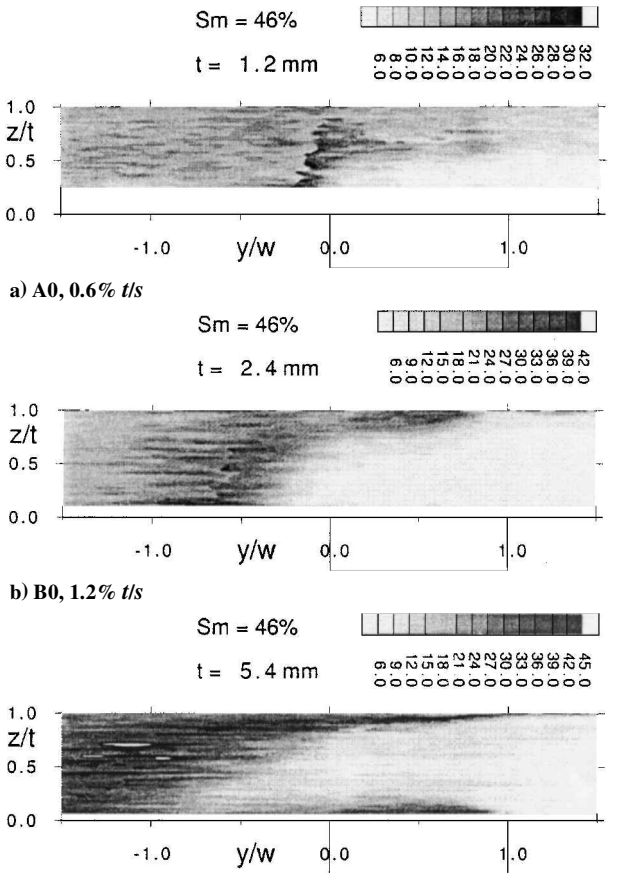


**Fig. 10 Contours of rms as a percentage of local blade tip speed determined from hot-wire measurements at 46% $S_m$.**

at low values of rms makes its way up to about $0.4y/w$, before it begins to mix with the scraping fluid from the top and the boundary layer of the blade tip surface from underneath. At gap exit ($y/w = 0$) the region of high rms values indicates the interaction between the tip leakage flow and the scraping flow outside the gap (the blocking effect of scraping). The mixing region due to the blocking effect coincides with the location of the dividing stream surface at gap exit as observed in Fig. 8a.

For the bigger gaps B0 and B8, Figs. 10b and 10c indicate a large portion of low rms tip leakage flow, and at least part of this low-turbulence fluid makes its way to the gap exit. The mixing regions inside the gap (due to the dragging effect) and at gap exit (due to the blocking effect) are more intense compared to the smaller gap A0. It is believed that this is due to a stronger tip leakage flow momentum as observed in Fig. 9. Figure 10c also indicates that the mixing region near the blade tip surface becomes more important for a bigger gap size. This could be due to the effect of the pressure side corner radius to tip gap height ratio, which is about 4.5 times smaller for gap B8 compared to gap A0 (see Heyes et al.[15]). In summary, Fig. 10 gives yet another piece of evidence that the tip leakage flow behavior for gap A0 is different from that for gaps B0 and B8.

### Different Tip Leakage Flow Behavior as a Function of Gap Height: Explanation

This section attempts to explain why the interaction between the tip leakage flow and the dragged fluid near the casing is different for gap A0 compared to the larger gaps B0 and B8. To do so, a few published results that were obtained under stationary, incompressible conditions are briefly reviewed. The one by Rains,[14] who examined the pressure at the casing for different tip gap height to width ratios $\lambda$, remains a very relevant work. His measurements were performed using a two-dimensional hydrofoil in a water tunnel without a moving endwall. Based on the experimental results, Rains[14] concluded that inertia effects inside the gap are dominant for $\lambda > \frac{1}{6}$ and that a potential flow pressure distribution is established at that ratio.

Reporting on cascade measurements, Bindon[16] showed that the tip leakage flow at exit may not be completely mixed out, but can consist in part of an isentropic jet. On the basis of these experiments, Heyes et al.[15] proposed their partial mixing model for tip leakage flow in axial turbomachinery and suggested that the amount of mixing achieved inside the gap depends on the Reynolds number of the tip leakage flow and on the tip gap height to width ratio $\lambda$. Based on results by Lichtarowicz et al.,[17] who investigated the variation of orifice discharge coefficients with orifice length, they[15] assumed that the mixing of the tip leakage would take place after the vena contracta between $1.5t$ and $6t$. Hence, according to Heyes and Hodson,[18] complete mixing of the tip leakage flow inside the gap only occurs for gap configurations of $\lambda < \frac{1}{6}$. Their findings and the results of Rains[14] suggest that the value $\lambda_{\mathrm{crit}} = \frac{1}{6}$ is a threshold for viscous effects inside the tip gap of a stationary cascade.

The relevant values of $\lambda$ for the present investigation are summarized in Table 2. It is not known how the relative casing motion affects the critical value of $\lambda$. However, the different behavior of tip leakage flow and scraping flow for the gap A0 may occur because $\lambda$ is smaller than $\lambda_{\mathrm{crit}}$ for both the inducer and the midsection, that is, for $0 < S_m < 60\%$, where a varying gap height makes a difference to the tip leakage flow pattern.

Figure 11 shows the two situations, that is, $\lambda < \lambda_{\mathrm{crit}}$ and $\lambda > \lambda_{\mathrm{crit}}$. In the case where $\lambda$ is smaller than $\lambda_{\mathrm{crit}}$, the entire tip leakage jet mixes with the scraping flow (complete mixing). Hence, the scraping

**Table 2 Values of $\lambda$ for different gap configurations**

| | $S_m$ | | | | |
|---|---|---|---|---|---|
| Gap | 9% | 21% | 34% | 46% | 58% |
| A0 | 0.146 | 0.125 | 0.116 | 0.144 | 0.155 |
| B0 | 0.208 | 0.230 | 0.265 | 0.292 | 0.322 |
| B8 | 1.203 | 1.125 | 0.901 | 0.651 | 0.549 |

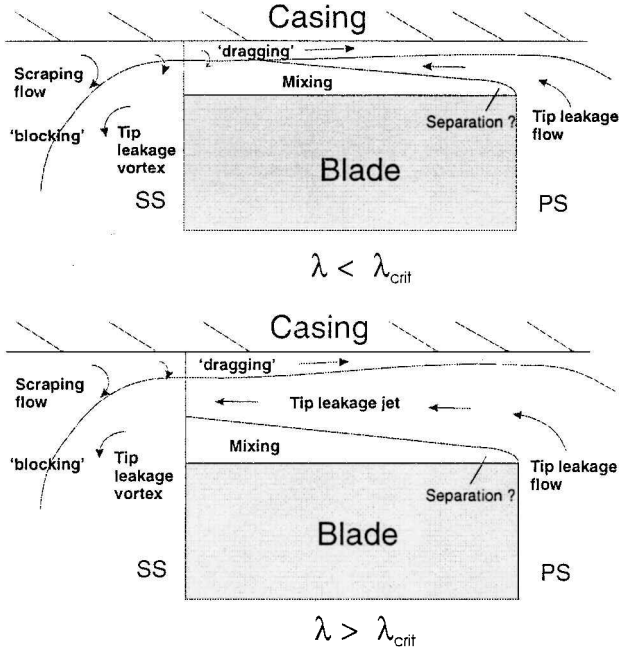


**Fig. 11 Schematic of tip leakage flow behavior for different values of λ.**

flow that enters the gap from the suction side is in contact with low-momentum fluid for some distance into the gap. In the case where $\lambda$ is larger than $\lambda_{crit}$, the tip leakage flow only partially mixes with the neighboring scraping flow, and the boundary layer on the blade tip surface remains distinct (partial mixing). In this case, the scraping flow is always in contact with the high-momentum tip leakage jet.

It appears from Fig. 11 that the ratios of $\lambda$ and $R$ are parameters that need to be taken into account for modeling purposes. Table 2 suggests a critical value of $\lambda$ in the range between $\frac{1}{6}$ and $\frac{1}{5}$ for the rotating case. It is possible that the tip leakage jet would experience full mixing for higher values of $\lambda$ in the rotating case because the scraping flow partially blocks the tip gap. Hence, for low values of $R$, ratio $\lambda_{crit}$ might be higher for the rotating case compared to the stationary case.

### Tip Leakage Mass Flow

Tip leakage mass flow at tip gap exit consists of pressure-driven tip leakage flow and scraping flow. The tip gap mass flow can be obtained by integrating the relative normal velocity profile over the height of the gap. The velocity at the blade tip surface is set equal to the nearest measured velocity inside the gap. The pressure-driven tip gap mass flow at gap exit was calculated using

$$\dot{m}_{tf} = S_{tip} \int_0^{z_0} \rho v_n \, dz \tag{5}$$

where $z = 0$ is at the blade tip surface, $z = z_0$ is the height where the blade normal velocity is equal to zero, and $S_{tip}$ is the blade length at the blade tip. Equally the scraping flow could be calculated using

$$\dot{m}_{sf} = S_{tip} \int_{z_0}^{t} \rho v_n \, dz \tag{6}$$

Figure 12 shows integrated values of scraping flow (as a percentage of passage mass flow) for all four gap configurations. The passage mass flow rate per unit meridional chord for all of the tests described here corresponds to 700 g/ms. The amount of scraping flow that passes from the suction side to the pressure side decreases almost linearly toward the midchord. Essentially no more scraping flow passes through the gap from about 40% $S_m$ downstream for all gap configurations. It appears that a relatively constant amount

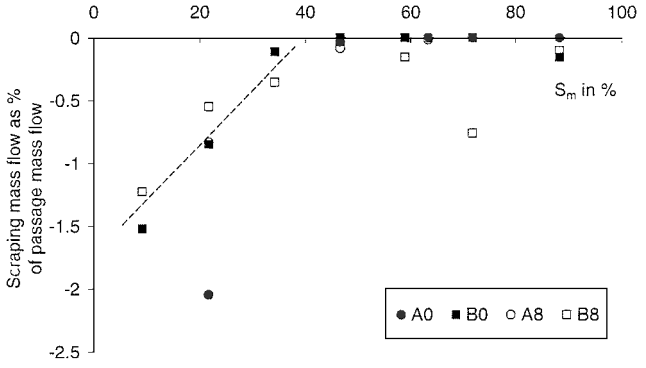


**Fig. 12 Integrated scraping mass flow rates from hot-wire measurements.**

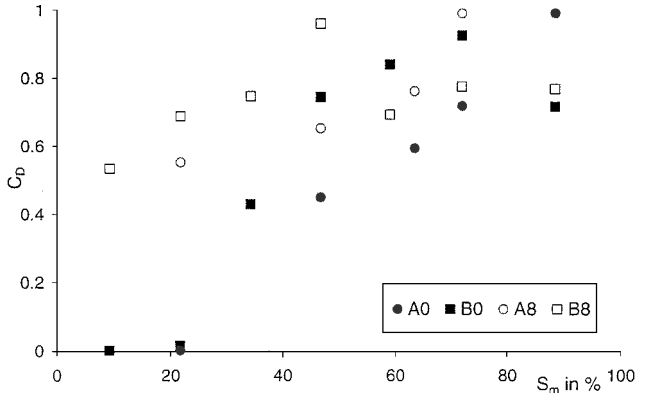


**Fig. 13 Discharge coefficient at tip gap exit for different gap configurations.**

of scraping flow is dragged through the gap independent of the gap height provided $\lambda$ is greater than $\lambda_{crit}$.

Figure 13 shows an experimentally determined discharge coefficient for pressure-driven tip leakage flow for each of the four gap heights. The discharge coefficient is defined as the ratio of the actual pressure-driven mass flow at gap exit divided by the ideal tip gap mass flow as follows:

$$C_D = \frac{\dot{m}_{tf}}{S_{tip} t \sqrt{2(\Delta p/\rho)}} \tag{7}$$

The measured pressure difference over the tip $\Delta p$ was calculated between the maximum and minimum pressure at the casing (see Fig. 5). The preceding definition of the discharge coefficient can also be seen as a measure of the viscous effects on the tip gap mass flow in a radial turbine.

In the inducer and the midsection (between 0% $S_m$ and 60% $S_m$), Fig. 13 confirms that the scraping effect significantly reduces the discharge coefficient for the small gap A0 and the medium gap B0. Results for gaps A8 and B8 indicate larger values of $C_D$ in the inducer and the midsection compared to the gaps A0 and B0. This is because the scraping effect occupies a relatively small part of the large clearance height, and its effect on the pressure driven mass flow is much reduced. If it can be assumed that tip leakage loss is proportional to the discharge coefficient (see Yaras and Sjolander[7]), Fig. 13 suggests that the scraping effect reduces tip leakage loss near the inducer. Hence, the blade tip speed and the local camber angle are important parameters if tip leakage loss in radial inflow turbines is in any way to be predicted.

## Conclusions

The present study has shown that the driving pressure difference over the gap remains relatively constant for a large variation of the gap height. This is an important result for modeling the tip gap flow with numerical tools. It also means that an inviscid pressure

difference can be used in a future tip gap mass flow or tip leakage loss model for radial turbines.

The nature of tip leakage flow in a radial turbine was found to be different depending on the tip gap height-to-width ratio $\lambda$. The measurements in the gap region of the inducer have revealed that a relatively constant amount of scraping flow is dragged through the gap for different gap heights, once the critical value of $\lambda$ is exceeded. If the gap height is small enough, the entire gap is occupied with scraping flow. The measurements in the gap region of the midsection have shown that the tip leakage flow mixes with the neighboring scraping flow and the boundary layer on the blade tip surface inside the gap. Full mixing occurs if $\lambda$ is below the critical value, and partial mixing occurs if $\lambda$ is above the critical value. The critical value of $\lambda$ appears to be close to the value reported for stationary cascade results, for example, $\lambda_{crit} \sim \frac{1}{6}$.

The discharge coefficient at gap exit has been quantified for four different clearance configurations. The scraping effect reduces the discharge coefficient in the inducer and to some extent in the midsection of the radial turbine for all four gap configurations. Consequently, the scraping flow is an important parameter to determine the tip gap discharge coefficient and, hence, tip gap loss in radial inflow turbines.

## Acknowledgments

The authors wish to thank Ishikawajima-Harima Heavy Industries, Japan, for their support of this project. The first author is thankful for being supported by the Swiss National Science Foundation and would like to acknowledge a grant from a foundation set up by ASEA Brown Boweri Switzerland. The authors would also like to thank T. Chandler and B. Taylor for their technical assistance.

## References

[1]Futral, S. M., and Holeski, D. E., "Experimental Results of Varying the Blade-Shroud Clearance in a 6.02-inch Radial Inflow Turbine," NASA TN D-5513, 1970.

[2]Ishino, M., Otuka, M., Uchida, H., and Sugiyama, K., "The Effects of Tip Clearance on Small Radial Turbine Perfomances," *Proceedings of the Yokohama International Gas Turbine Congress*, Vol. 3, 1991, pp. 165–169.

[3]Jones, A. C., "Design and Test of a Small, High Pressure Ratio Radial Turbine," *Journal of Turbomachinery*, Vol. 118, No. 2, 1996, pp. 362–370.

[4]Japikse, D., and Baines, N. C., *Introduction to Turbomachinery*, 1st ed., Concepts NREC, White River Junction, VT, 1994, pp. 7–17.

[5]Sjolander, S. A., "Overview of Tip-Clearance Effects in Axial Turbines," Secondary and Tip-Clearance Flows in Axial Turbines, VKI Lecture Series 1997–01, pp. 1–24, 1997, von Kármán Inst. for Fluids Dynamics, Rhode Saint Genèse, Belgium.

[6]Dambach, R., Hodson, H. P., and Huntsman, I., "An Experimental Study of Tip Clearance Flow in a Radial Inflow Turbine," *Journal of Turbomachinery*, Vol. 121, No. 4, 1999, pp. 644–650.

[7]Yaras, M. I., and Sjolander, S. A., "Prediction of Tip-Leakage Losses in Axial Turbines," *Journal of Turbomachinery*, Vol. 114, No. 1, 1992, pp. 204–210.

[8]Kaiser, I., and Bindon, J. P., "The Effect of Tip Clearance on the Development of Loss Behind a Rotor and a Subsequent Nozzle," American Society of Mechanical Engineers, ASME Paper 97-GT-53, 1997.

[9]Huntsman, I., and Hodson, H. P., "A Laminar Flow Rotor for a Radial Inflow Turbine," AIAA Paper 93-1796, 1993.

[10]Huntsman, I., and Hodson, H. P., "An Experimental Assessment of the Aerodynamic Performance of a Low-Speed Radial Inflow Turbine," AIAA Paper 94-2932, 1994.

[11]Roelke, R. J., and Rogo, C., "Experimental Evaluation of a Translating Nozzle Sidewall Radial Turbine," NASA TM 88963, 1987.

[12]Sjolander, S. A., and Amrud, K. K., "Effects of Tip Clearance on Blade Loading in a Planar Cascade of Turbine Blades," *Journal of Turbomachinery*, Vol. 109, No. 2, 1987, pp. 237–244.

[13]Bindon, J. P., "Pressure Distributions in the Tip Clearance Region of an Unshrouded Axial Turbine as Affecting the Problem of Tip Burnout," American Society of Mechanical Engineers, ASME Paper 87-GT-230, 1987.

[14]Rains, D. A., "Tip Clearance Flows in Axial Flow Compressors and Pumps," Rept. 5, California Inst. of Technology, Hydro and Mech. Eng. Labs., Pasadena, CA, June 1954.

[15]Heyes, F. J. G., Hodson, H. P., and Dailey, G. M., "The Effect of Blade Tip Geometry on the Tip Leakage Flow in Axial Turbines," *Journal of Turbomachinery*, Vol. 114, No. 3, 1992, pp. 643–651.

[16]Bindon, J. P., "The Measurement and Formation of Tip Clearance Loss," *Journal of Turbomachinery*, Vol. 111, No. 2, 1989, pp. 257–263.

[17]Lichtarowicz, A., Duggins, R. K., and Markland, E., "Discharge Coefficients for Incompressible Non-Cavitating Flow Through Long Orifices," *Journal of Mechanical Engineering Science,* Vol. 7, No. 2, 1965, pp. 210–219.

[18]Heyes, F. J. G., and Hodson, H. P., "The Measurement and Prediction of the Tip Clearance Flow in Linear Turbine Cascades," *Journal of Turbomachinery*, Vol. 115, No. 2, 1993, pp. 376–382.